European Journal of Cell Biology 101 (2022) 151185

Contents lists available at ScienceDirect

European Journal of Cell Biology

journal homepage: www.elsevier.com/locate/ejcb

Cannabidiol activates PINK1-Parkin-dependent mitophagy and mitochondrial-derived vesicles

Adrian Ramirez [a,b], William Old [a,b], David L. Selwood [c], Xuedong Liu [a,*]

[a] Department of Biochemistry, University of Colorado, Boulder, CO 80303, USA
[b] Department of MCD-Biology, University of Colorado, Boulder, CO 80309, USA
[c] Wolfson Institute for Biomedical Research, University College London, Gower Street, WC1E6AE, United Kingdom

ARTICLE INFO

Keywords:
Cannabidiol
Mitochondrial-derived vesicles (MDV)
Mitophagy
Mitochondrial quality control
Parkin
PINK

ABSTRACT

The PINK1/Parkin pathway plays an important role in maintaining a healthy pool of mitochondria. Activation of this pathway can lead to apoptosis, mitophagy, or mitochondrial-derived vesicle formation, depending on the nature of mitochondrial damage. The signaling by which PINK/Parkin activation leads to these different mitochondrial outcomes remains understudied. Here we present evidence that cannabidiol (CBD) activates the PINK1-Parkin pathway in a unique manner. CBD stimulates PINK1-dependent Parkin mitochondrial recruitment similarly to other well-studied Parkin activators but with a distinctive shift in the temporal dynamics and mitochondrial fates. The mitochondrial permeability transition pore inhibitor cyclosporine A exclusively diminished the CBD-induced PINK1/Parkin activation and its associated mitochondrial effects. Unexpectedly, CBD treatment also induced elevated production of mitochondrial-derived vesicles (MDV), a potential quality control mechanism that may help repair partial damaged mitochondria. Our results suggest that CBD may engage the PINK1-Parkin pathway to produce MDV and repair mitochondrial lesions via mitochondrial permeability transition pore opening. This work uncovered a novel link between CBD and PINK1/Parkin-dependent MDV production in mitochondrial health regulation.

1. Introduction

A healthy pool of mitochondria is vital to normal cell physiology. Dysregulation in mitochondrial maintenance and signaling has been linked to a myriad of diseases, including cancer, cardiovascular disease, and neurodegenerative diseases (Boland et al., 2013; Chistiakov et al., 2017; Yeung et al., 2021). A subset of familial Parkinson's disease patients harbor mutations to several mitochondrial genes (Klein and Westenberger, 2012), including *PINK1* and *PRKN*. The PINK1 and Parkin proteins are required for initiating the degradation of damaged mitochondria through mitophagy or induction of mitochondrial-derived vesicles (MDV) to target damaged proteins and lipids to lysosomes (Pickrell and Youle, 2015; Sugiura et al., 2014). The significance and relative contribution of these two mechanisms of PINK1-Parkin-dependent mitochondrial quality control to Parkinson's disease are yet to be fully understood.

Parkin, an E3 ubiquitin ligase, and PINK1, a serine-threonine protein kinase, regulate mitochondrial homeostasis during specific stress events (Pickrell and Youle, 2015). In cells with healthy and polarized mitochondria, PINK1 is constantly transported through the outer mitochondrial membrane (OMM) to the inner mitochondrial membrane (IMM), where it is cleaved and consequently degraded (Greene et al., 2012; Jin et al., 2010). When mitochondria sustain certain injuries like depolarization, PINK1 import to mitochondria stalls, and PINK1 is no longer cleaved or degraded (Matsuda et al., 2010; Narendra et al., 2010). As a result, PINK1 accumulates and stabilizes on the OMM of damaged mitochondria, where it phosphorylates both ubiquitin and Parkin, recruiting Parkin to these specific damaged mitochondria (Pickrell and Youle, 2015). Upon recruitment, Parkin ubiquitinates target proteins on the OMM, which leads to recruitment of autophagosome machinery, engulfment of the damaged mitochondria, and subsequent degradation of mitochondria via lysosomes (Ordureau et al., 2020; Yoshii et al., 2011).

Parkin's ubiquitination profile and the signaling parade leading to

Abbreviations: CBD, cannabidiol; MDV, mitochondrial-derived vesicles; CypD, cyclophilin D; MPTP, mitochondrial permeability transition pore; AO, Antimycin A and Oligomycin A; CsA, cyclosporine A.

* Corresponding author.
E-mail address: Xuedong.Liu@colorado.edu (X. Liu).

https://doi.org/10.1016/j.ejcb.2021.151185
Received 14 July 2021; Received in revised form 27 October 2021; Accepted 12 November 2021
Available online 14 November 2021

mitophagy have been well characterized (Sarraf et al., 2013; Yamano et al., 2016). While mitophagy is the most studied outcome from this signaling pathway in mammalian cells, PINK1/Parkin activity at damaged mitochondria can also selectively induce apoptosis or MDVs depending on stimuli and levels of mitochondrial damages (Carroll et al., 2014; McLelland et al., 2014; Zhang et al., 2014). Other than elevated ROS production in general, few if any specific physiologically relevant input signals have been identified for stimulation of MDVs (Roberts et al., 2016).

Cannabidiol (CBD) and CBD-derived compounds have long garnered interest as a treatment for a broad range of disorders. Successful clinical trials led to the recent approval of CBD for Dravet syndrome and Lennox-Gastaut Syndrome, two rare childhood epileptic disorders (Devinsky et al., 2017; Thiele et al., 2018). This spurred additional clinical trials into other diseases, such as Parkinson's disease (Leehey et al., 2020). Despite these promising clinical results, the molecular mechanisms of action for CBD's therapeutic benefits remains elusive.

With mitochondrial dysfunction implicated in neurodegenerative diseases, the powerhouse of the cell provides an interesting target for CBD research. CBD has been reported to disrupt mitochondrial calcium homeostasis in Jurkat cells treated above 30 μM, leading to increased cytosolic calcium and cell death (Olivas-Aguirre et al., 2019). 10 μM CDB induced mitochondrial swelling in BV2 glial cells while 50 μM impaired the mitochondrial complex activity of isolated mitochondria (Rimmerman et al., 2013; Singh et al., 2015). However, other studies reported conflicting outcomes in the same dose range, with CBD causing improved mitochondrial health in both isolated mitochondria and mouse cardiac tissue while also increasing cell viability in the cardiac tissue (Hao et al., 2015; Valvassori et al., 2013). In light of these seemingly contradictory studies, further research is required to clarify the effect of CBD on mitochondrial fitness.

Here we investigated the effect of CBD on mitochondrial quality control. We discovered that CBD activates the PINK1/Parkin pathway in a dose-dependent manner. We determined that CBD shares some characteristics with established PINK1/Parkin activator Antimycin A and Oligomycin A (AO), inducing mitochondrial depolarization, ROS production, and mitophagy. These downstream effects of CBD, but not AO or CCCP, are blocked by cyclosporine A, an inhibitor of calcineurin and the mitochondrial permeability transition pore (MPTP), or knockdown of cyclophilin D (CypD). CBD also causes elevated generation of mitochondria derived vesicles, suggesting that a novel mechanism of action for this drug. The difference between CBD and CCCP or AO points to a novel mechanism of PINK1/Parkin activation by CBD which could help inform future clinical relevance of the drug in treating neurodegenerative diseases such as Parkinson's disease.

2. Results

2.1. CBD induces Parkin recruitment to mitochondria

Previous studies have demonstrated that Parkin translocates to mitochondria when cells are treated with compounds that inhibit mitochondrial function. Such inhibitors include the protonophore carbonyl cyanide m-chlorophenyl hydrazone (CCCP), potassium ionophore Valinomycin, or dual inhibition of complex III and V of the electron transport chain by Antimycin A and Oligomycin A (AO) or sorafenib (Narendra et al., 2008; Vives-Bauza et al., 2010; Zhang et al., 2017, 2014). Other studies have shown that CBD also inhibits mitochondrial complex activity (Singh et al., 2015). We thus decided to test if the mitochondrial stress caused by CBD treatment was sufficient to induce Parkin recruitment. We employed HeLa cells expressing Venus-Parkin and mitochondrial targeted RFP containing a mitochondrial targeting sequence from Smac fused to RFP referred hereafter as Smac-MTS-RFP. The double-labeled HeLa cells were treated with compounds and then imaged. Venus and RPF colocalization was quantified using Pearson's Correlation Coefficient (PCC). Cells treated with 50 μM CBD exhibit a strong Parkin colocalization to mitochondria compared to vehicle-treated cells (Fig. 1A). However, the dynamics of CBD-induced activation of Parkin appears to differ from AO. CBD induced a lower maximal Parkin translocation at 6 h compared to AO at 2 h (Fig. 1B). To further affirm Parkin mitochondrial recruitment, we also tested how Parkin colocalized to endogenous outer mitochondrial protein Tom20. We treated cells expressing Venus-Parkin with AO, CBD or vehicle control for 2, 6, and 6 h, respectively, then fixed and immunostained for Tom20. CBD and AO caused Parkin colocalization to Tom20 compared to vehicle treated cells, verifying what we saw with Smac-MTS-RFP (Fig. S1A and B).

To determine whether the CBD effect on Parkin is cell line-specific, Parkin puncta formation was compared in HeLa, RPE1, beige fat cells, and mouse embryonic fibroblast (MEF) cells that express Venus-Parkin. As seen in Fig. S2A–C and quantified in Fig. S2D–F, all three cell lines show Parkin puncta formation, though it should be noted that the inguinal cells require 10 h to demonstrate levels of Parkin recruitment seen after only 6 h in HeLa and RPE1 cell lines. HeLa, RPE1 and the inguinal fat cells shared similar maximal Parkin puncta formation EC_{50} (26.6, 28.0 and 26.1 μM, respectively) (Fig. S1G–J).

2.2. CBD stabilizes PINK1 required for Parkin recruitment

PINK1 stabilization in response to damaged mitochondria is associated with Parkin mitochondrial recruitment (Narendra et al., 2010). To investigate whether CBD also induces PINK1 stabilization, we first measured PINK1 levels in HeLa cells stably expressing PINK1-EGFP. Under basal conditions, PINK1 is constantly being produced and subsequently degraded, leading to low levels of detectable PINK1, as seen in vehicle-treated control cells (Fig. 2C and D, yellow line). Cells treated with 10 μM AO showed an increase in PINK1-EGFP due to the halt of PINK1 import and degradation (Fig. 1C) that increases over time (Fig. 1D, red line). As expected, 50 μM CBD also increases PINK1-EGFP expression (Fig. 1C). Much like with Parkin recruitment, the CBD-induced PINK1 effects lag in comparison to AO (Fig. 1D, blue line).

Next, we tested whether PINK1 is required for Parkin recruitment to mitochondria in CBD-treated cells. MEF cells with PINK1 knocked out (PINK1-/-) were stably transduced with Venus-Parkin and PINK1-M318A, which have a mutation in the gatekeeper residue that makes the kinase catalytic activity sensitive to inhibition by 1-NA-PP1, while preserving its catalytic activity to wild-type levels with ATP (Zhang et al., 2015). When these MEF cells are treated with 10 μM AO or 50 μM CBD, they demonstrate Parkin mitochondrial translocation as expected (Fig. 1E, upper panels), with a delayed response in CBD-treated cells compared to AO-treated cells. When cells are treated with 5 μM 1-NA-PP1 in conjunction with AO or CBD, Parkin recruitment is abrogated completely (Fig. 1E, lower panels). When we quantified the amount of Parkin puncta formation generated, we can see that CBD and AO cause an increase compared to vehicle treated cells (Fig. 1F, blue bars). Addition of 1-NA-PP1 significantly decreased the quantifiable Parkin puncta from CBD and AO (Fig. 1F, orange bars). Thus, PINK1 kinase activity is required for CBD-induced Parkin recruitment.

2.3. The effects of CBD on mitochondrial polarization, ROS production, and degradation

Depolarizing mitochondria is a shared characteristic among many of the Parkin activating agents including CCCP, valinomycin, and AO (Narendra et al., 2008; Vives-Bauza et al., 2010; Zhang et al., 2014). However, some treatments such as actinonin or overexpression of truncated ornithine transcarbamylase (OTC) cause Parkin localization while not significantly altering mitochondria membrane potential (Burman et al., 2017). To test whether CBD affects mitochondrial membrane potential, HeLa cells were incubated with tetramethylrhodamine, ethyl ester (TMRE), a dye that localizes to polarized cells but diffuses when that potential decreases. When these cells are treated with

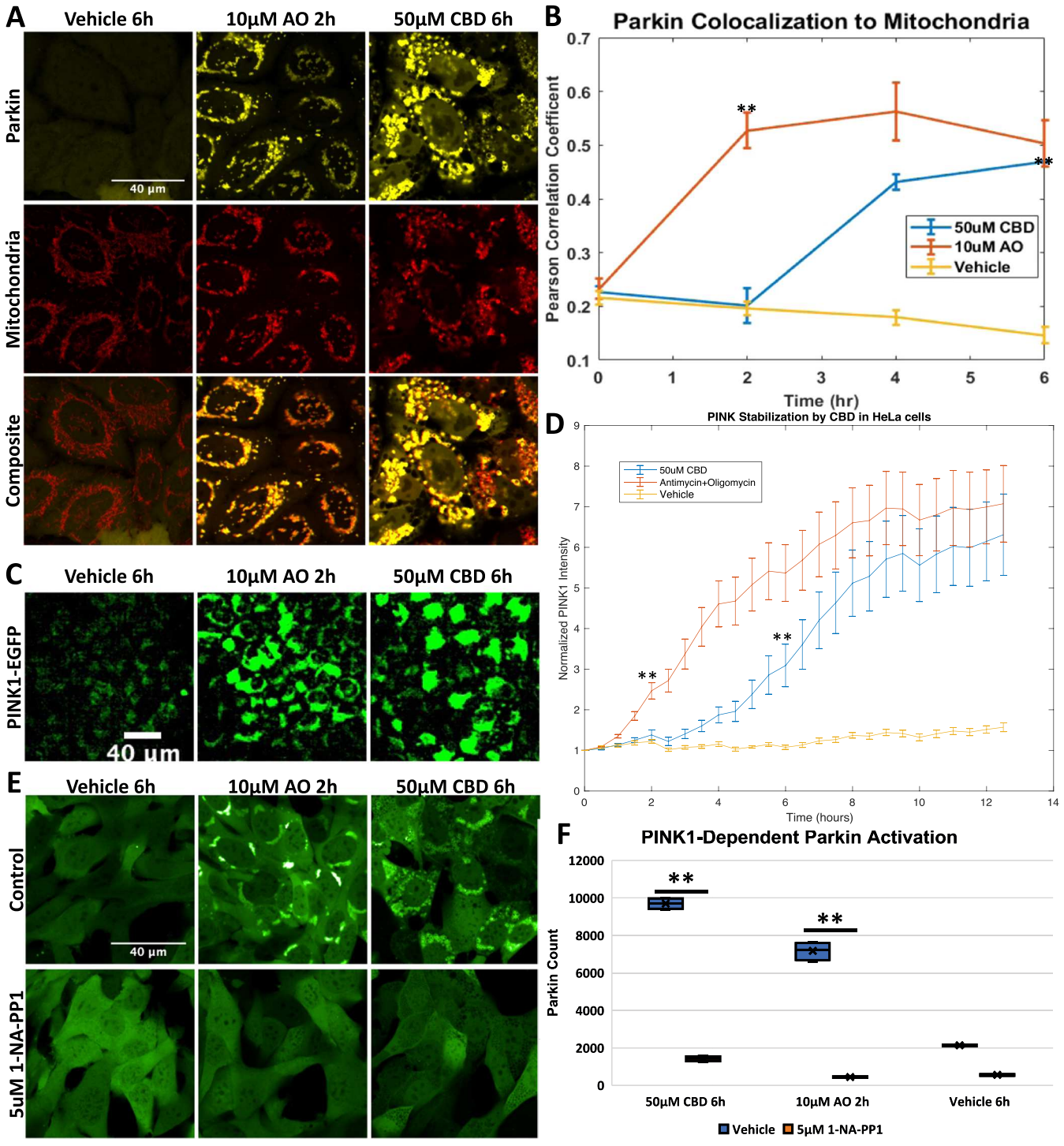

Fig. 1. CBD causes Parkin localization and PINK1 stabilization, A. HeLa Venus-Parkin Smac-MTS-RFP were treated with either DMSO vehicle control, 10 μM Antimycin and Oligomycin (AO), or 50 μM CBD for indicated amount of time and imaged for YFP and mCherry signal, B. Pearson's colocalization coefficient between Smac-MTS-RFP and Venus-Parkin was measured to quantify colocalization of Parkin to mitochondria. Error bars represent SD, *t*-test results comparing vehicle and drug treatment represented as p-value < .005 = **, n = 3, C. HeLa PINK1-EGFP cells were treated with 50 μM CBD, 10 μM AO or Vehicle control and then imaged every 30 min. Representative images of PINK1-EGFP accumulation from mitochondrial damage shown, D. Quantification of PINK1 accumulation quantified by measuring EGFP signal intensity and normalizing to initial EGFP determined for each condition. Error bars represent SD, *t*-test results comparing vehicle and drug treatment represented as p-value < .005 = **, n = 3, E. MEF Venus-Parkin PINK1-/- PINK1-M318A cells were initially treated with Vehicle or 5 μM 1-NA-PP1 for 20 min. Cells were then treated with either Vehicle, 10 μM AO or 50 μM CBD for indicated amount of time, then imaged for Venus-Parkin puncta formation, F. Quantification of Parkin Recruitment by puncta formation. *t*-test results comparing vehicle and 1-NA-PP-1 treated cells represented as p-value < .005 = **, n = 4.

AO, there is an immediate decrease in TMRE intensity compared to vehicle treated cells, with TMRE intensity reaching a minimum at 40 min (Fig. 2A, AO orange line, Vehicle cyan line). Cells treated with 50 μM CBD also causes a significant decrease in TMRE intensity, but interestingly this effect is not immediate as seen with AO (Fig. 2A, purple line). This decrease in membrane potential is delayed by an hour,

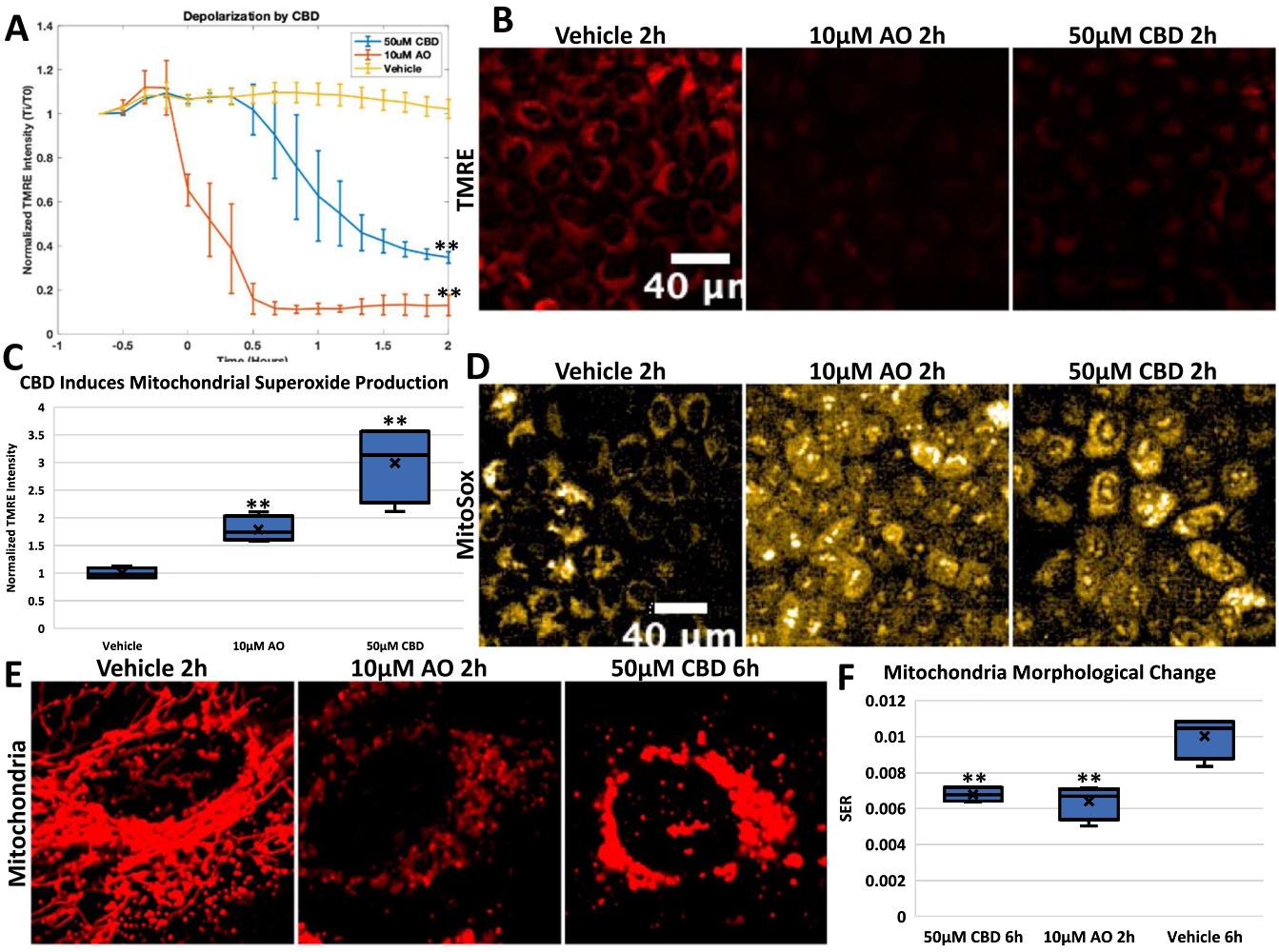

Fig. 2. CBD depolarizes and perturbs architecture of mitochondria. A. HeLa cells were stained with TMRE dye and then treated with Vehicle control, 10 µM AO, or 50 µM CBD. TMRE signal imaged every 10 min, and then quantified by normalizing at initial TMRE signal for each condition. Error bars represent SD, *t*-test comparing vehicle to drug treated represented as p-value < .005 = **, n = 3, B. Representative images of TMRE signal from HeLa cells treated with Vehicle, AO or 50uM CBD at 2 h, C. HeLa cells were stained with MitoSox dye and then treated with Vehicle control, 10 µM AO, or 50 µM CBD for the indicated times. MitoSox signal imaged at 2 h, stained for TOM20, and then quantified by normalizing for mitochondrial content. *t*-test comparing vehicle to drug treated represented as p-value < .005 = **, n = 4, D. Representative images of MitoSox signal from HeLa cells treated with Vehicle, 10 µM AO or 50uM CBD at 2 h, E. HeLa Venus-Parkin Smac-MTS-RFP cells treated with DMSO, 10uM AO or 50uM CBD and then imaged for Smac-MTS-RFP signal. Time of each treatments indicated, F. Quantification of mitochondria morphological change with drug at specified time using SER texture analysis on the Harmony analysis software suite and represented using box plots. Briefly, SER measures the intensity patterns to different textures; here pixels were measured for patterns related to 'holes'. With healthy networked mitochondria, holes appear around the filamentous signal; in damaged mitochondria, these 'holes' appear less strongly and is shown thus in the analysis. *t*-test comparing vehicle to drug treated represented p-value < .005 = **.

after which mitochondria then proceed to depolarize similarly to AO-treated cells. This indicates that the mitochondrial depolarization that causes Parkin recruitment is not occurring instantaneously after CBD treatment, suggesting that CBD is causing a change in cell metabolism or membrane lipid composition that takes time to affect mitochondrial function.

Inhibition of complexes III and V by AO causes generation of ROS at the mitochondria that can cause harmful localized damage. Because CBD causes mitochondrial depolarization, we investigated whether CBD also causes generation of ROS at the mitochondria. HeLa cells were stained with MitoSox, a mitochondria-targeted red dye that increases in intensity in the presence of superoxide. While the vehicle control induced no change in MitoSox signal, AO caused a significant increase in superoxide production over time (Fig. 2C, AO orange line, DMSO light blue line, Fig. 2D). 50 µM CBD also led to a significant increase in MitoSox signal, but at a lower level compared with AO during the times tested (Fig. 2C, 50 µM CBD green line, Fig. 2D).

Next, we determined the effects CBD on mitochondrial morphology. First, we assessed what effects CBD had on the gross morphology of mitochondria. HeLa cells with Venus-Parkin and Smac-MTS-RFP were treated with vehicle, AO, or CBD, and then imaged for mitochondria signal over time. As shown, vehicle-treated mitochondria stay networked, whereas AO-treated cells show clear fragmentation of mitochondria after 2 h (Fig. 2E, left and middle panel, respectively). Much like with Parkin recruitment, CBD-treated cells demonstrate a change to mitochondria morphology that occurs later compared to a similar morphology change in AO-treated cells (Fig. 2E). CBD treated mitochondria are also fragmenting but appear swollen compared to AO. This difference could also point to differences in their mitochondria damaging effects. To quantify this, we measured the SER (Saddle, Edges, Ridges) feature 'holes' of these images using the PerkinElmer Harmony software. Briefly, SER features scores the intensity of local pixels to determine a profile, with valley measuring how much the intensity drops off from each intense fluorescent locus. With the healthy network pattern of mitochondria seen in control cells, this leads to the highest value. Fragmentation of mitochondria, as observed in cells treated with

AO for 2 h, leads to a significant decreased SER "holes" value, indicating a change in mitochondrial morphology (Fig. 2F). When this analysis is applied to CBD-treated cells after 6 h, we see the same level of feature change as AO. Thus, CBD appears to have a direct effect on mitochondrial morphology and network.

2.4. CBD induces mitophagy and mitochondrial morphological change

Since AO-induced Parkin localization canonically leads to mitophagy, we asked whether CBD treatment would lead to this same outcome. One of the ways to test for mitophagy is by measuring the mitochondrial recruitment of autophagy marker LC3, a protein involved in autophagosome biogenesis. HeLa cells expressing Venus-Parkin, Smac-MTS-RFP and LC3-CFP were treated with Vehicle, AO, or CBD, and then imaged to determine if LC3 colocalization to damaged mitochondria would follow the Parkin colocalization shown above. As expected, Parkin translocation to mitochondria peaks at 2 h in AO-treated cells (Fig. 3A, 2nd row, Fig. 3C, red line), while CBD-treated cells take around 6 h to reach the same level of Parkin colocalization with mitochondria (Fig. 3B, 3rd row, Fig. 3C, blue line). We next quantified the PCC for cells treated with AO and CBD compared to vehicle control. AO-treated cells show an increase in LC3 signal overlapping with mitochondria puncta; this increase is most apparent at 6 h after treatment (Fig. 3A). PCC confirms that LC3 colocalization with mitochondrial puncta peaks at 7 h (Fig. 3D, red line). LC3 colocalization in CBD-treated cells also increases, though more subtly, with a more modest increase in LC3 puncta intensity (Fig. 3B), which is supported when quantified by PCC, with LC3 colocalization occurring later and reaching a lower level compared to in AO-treated cells (Fig. 3D, blue line). This delay of LC3 colocalization echoes the delayed Parkin localization in CBD-treated cells, giving further support that Parkin activity in CBD-treated cells is distinct from that in AO-treated cells.

We wanted to ensure that Parkin was required for the recruitment of LC3 to damaged mitochondria during CBD treatment. Parkin is known to be lowly expressed or not detectable in certain cell lines such as HeLa cells (Pawlyk et al., 2003). We thus employed HeLa cells expressing Smac-MTS-RFP and LC3-CFP, and compared cells with or without Venus-Parkin added in. Compared to cells without exogenous Parkin, Venus-Parkin expressing cells had an increase of LC3 colocalizing to mitochondria during CBD or AO treatment (Fig. S3). Vehicle treated cells showed no difference in LC3 colocalization to mitochondria between the two cell lines (Fig. S3). This result provides evidence that the recruitment of mitophagy machinery during CBD treatment requires Parkin.

We observed that CBD causes autophagosome machinery to colocalize to mitochondria, the first step in mitophagy (Fig. 3B&D). To

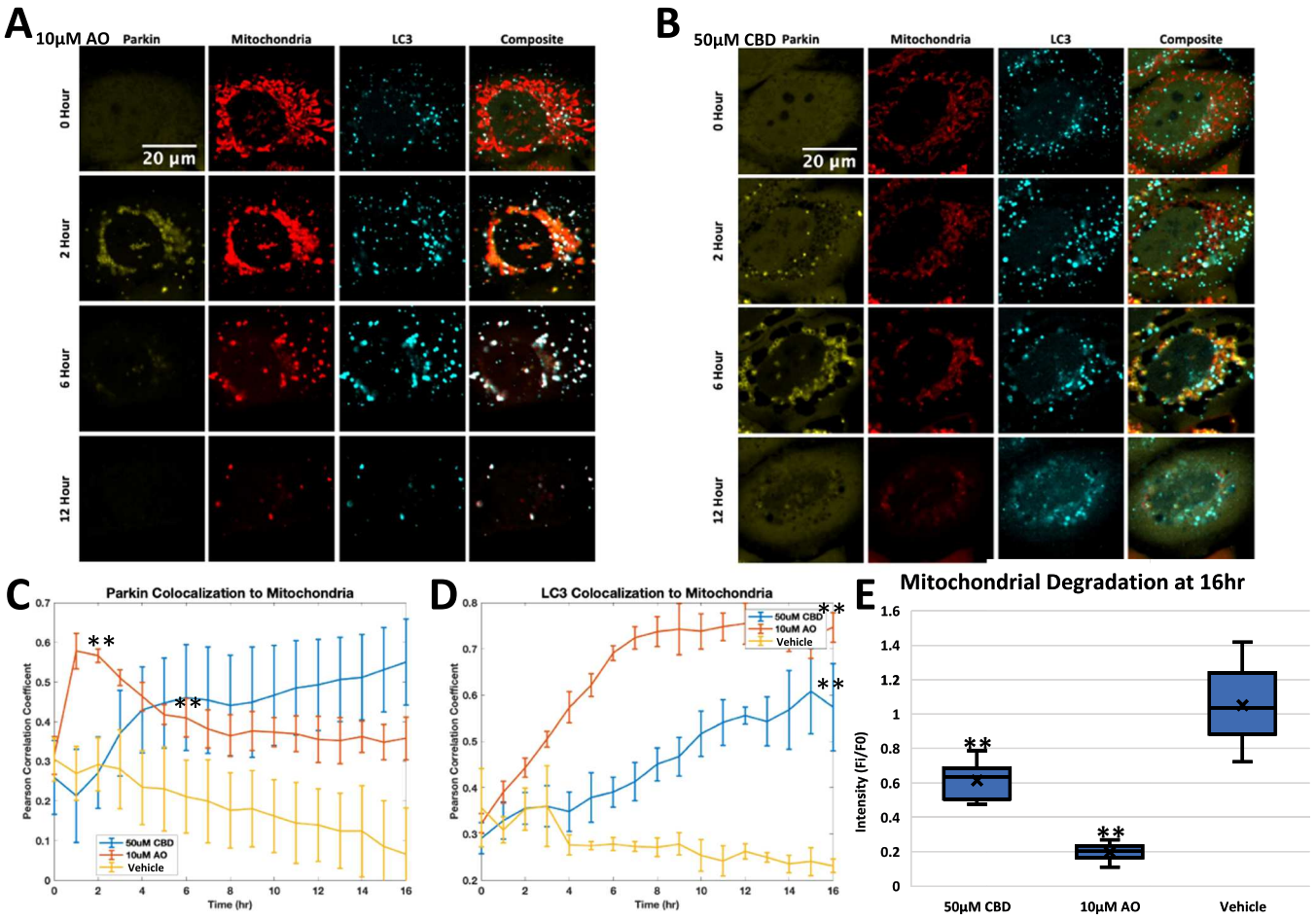

Fig. 3. CBD causes Parkin-dependent LC3 colocalization. A. HeLa cells were treated with 10 μM AO and then imaged for Venus-Parkin, Smac-MTS-RFP, and LC3-FFP every hour. Representative images at 0, 2, 6 and 12 h shown, B Same as (A) but with cells treated with 50 μM CBD, C. Quantification of Venus-Parkin colocalization to Smac-MTS-RFP using Pearson's Correlation Coefficient (PCC) of cells from (A) and (B) along with cells treated with Vehicle control. Error bar represent SD, *t*-test comparing vehicle to drug treated represented as p-value < .005 = **, n = 3, D. Quantification of LC3-CFP colocalization to Smac-MTS-RFP using Pearson's Correlation Coefficient (PCC) of cells from (A) and (B) along with cells treated with Vehicle control. Error bar represent SD, *t*-test comparing vehicle to drug treated represented as p-value < .005 = **, n = 3, E. Cells were treated for with 50 μM CBD, 10 μM AO or Vehicle, and imaged at 0 and 16 h for mitochondrial content as seen in (A). Smac-MTS-RFP intensity was calculated, and fold change of mitochondrial content was compared between 0 and 16 h. *t*-test comparing vehicle to drug treated represented as p-value < .005 = **, n = 10–11.

measure the loss of mitochondria directly, we measured mitochondrial content over time after drug treatment. Cells treated with 10 μM AO reduced initial mitochondrial signal to 19.6% after 16 h, as expected after mitochondria undergo mitophagy (Fig. 3E, middle bar). Cells treated with 50 μM CBD had 61.4% of their mitochondrial content remaining after 16 h, significantly less than vehicle treated, but still more than AO (Fig. 3E left bar). This blunted response is in line with the other CBD-induced effects presented above.

2.5. Cyclosporine A attenuates CBD-induced Parkin activity and cytotoxicity

After establishing that CBD differs from AO in temporal regulation of Parkin localization and mitochondrial impairment, we next investigated whether these differences engender varied phenotypical outcomes. Olivas-Aguirre, et al. showed that CBD caused cytotoxic defects to the mitochondrial derived calcium signaling in Jurkat cells and that these effects can be countered by cyclosporine A (CsA). CsA binds cyclophilin D, which can help form the mitochondrial permeability transition pore (MPTP) or inhibit calcineurin signaling (Olivas-Aguirre et al., 2019). We therefore tested CBD in the presence of CsA to determine whether CsA could inhibit Parkin activity too. HeLa cells with Venus-Parkin, Smac-MTS-RFP, and LC3-CFP were pretreated with either vehicle or CsA for 20 min, then CBD was added to the cells. As shown, CBD with a vehicle pretreatment causes a strong Parkin localization phenotype at 6 h (Fig. 4A, 3rd row), and caused an increase in both Parkin and LC3 colocalization to mitochondria along with stabilization of PINK1-EGFP (Fig. 4B, C and D, respectively, green line). When CsA was added to cells before CBD treatment, cells demonstrated a near complete reduction of Parkin colocalization after 6 h (Fig. 4A, 6th row). CsA also led to a decrease in CBD-induced Parkin and LC3 colocalization to the mitochondria and in PINK1 stabilization (Fig. 4B, C and D, respectively, cyan line). In contrast, cells treated with AO demonstrated Parkin mitochondrial translocation at 2h regardless of CsA presence (Fig. 4A, 4th row). Parkin and LC3 colocalization were also unaffected (Fig. 4B and C, cyan line), although we noted that CsA and AO in combination cause an increase to PINK1 stabilization compared to AO alone (Fig. 4D, AO+CsA cyan line, AO green line). We also employed FK506 to block calcineurin and Ru360 to block mitochondrial calcium uptake individually as CsA is known to block these two pathways in addition to MPTP. Unlike CsA, both FK506 and Ru360 failed to block Parkin recruitment caused by CBD (Fig. S4A). To confirm CsA is acting at the mitochondria, we employed JW47, a mitochondrial targeted CsA (Warne et al., 2016). In RPE1 cells, JW47 was able to significantly diminish CBD induced Parkin puncta formation, though to a lesser extent compared to what is seen with CsA (Fig. S4B). This result provides support that the inhibition exhibited by CsA is specific and predominately due to signaling at the mitochondria. The canonical target of CsA is cyclophilin D (CypD), so we also wanted to test if direct modulation of CypD would phenocopy CsA. We knocked down CypD using a short hairpin RNA (shRNA), with a non-targeting sequence (NT) shRNA used a control. We confirmed we successfully knocked down CypD expression by qPCR (Fig. S5A). The CypD knock down demonstrated a significant decrease in Parkin puncta formation with 100 μM CBD compared to cells transduced with NT (Fig. S5B). It should be noted that this inhibition occurred only at this higher dosage of CBD, which could be attributed to incomplete knockdown of CypD (Fig. S5A). Regardless, our data suggests that CypD is a key mediator of CBD. CsA selectively inhibited Parkin activity in CBD

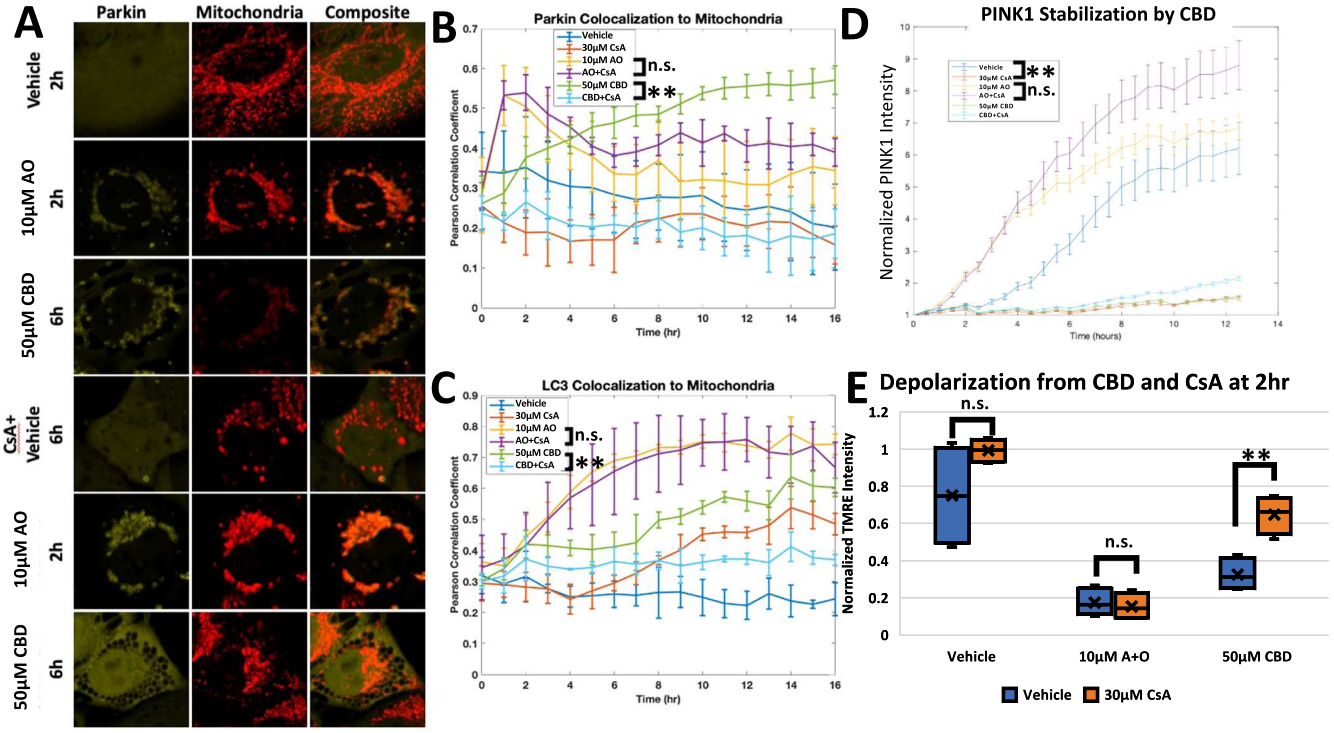

Fig. 4. MTP-Inhibitor Cyclosporine A blocks CBD Induced Parkin Activity. A. HeLa Venus-Parkin Smac-MTS-RFP LC3-CFP cells were initially treated with Vehicle or 30 μM CsA for 20 min. Cells were then treated with either Vehicle, 10 μM AO or 50 μM CBD and then imaged every hour. Representative images at indicated time points for Venus-Parkin and Smac-MTS-RFP shown, B. Colocalization of Venus-Parkin to Smac-MTS-RFP for each condition quantified with PCC. Error bars represent SD, *t*-test comparing vehicle to CsA pretreatment represented as p-value < .005 = **, n.s. = not significant, n = 3, C. Colocalization of LC3-CFP to Smac-MTS-RFP for each condition quantified with PCC. Error bars represent SD, *t*-test comparing vehicle to CsA pretreatment represented as p-value < .005 = **, n.s. = not significant, n = 3, D. PINK1 stabilization tested by treating initially with Vehicle or 30 μM CsA, then with Vehicle, 10 μM AO, or 50 μM CBD. PINK1-EGFP intensity measured and quantified by normalized to initial measurement. *t*-test results represented as p-value < .005 = **, n.s. = not significant, n = 3, E. Depolarization of mitochondria tested by treating initially with Vehicle (blue bars), 10 μM CsA (orange bars) or 30 μM CsA (gray bars) then with Vehicle, 10 μM AO, or 50 μM CBD. TMRE then measured and quantified by normalizing to initial measurement. *t*-test results represented as p-value < .005 = **, n.s. = not significant, n = 4.

treated cells but not AO treated cells, which indicates that distinct pathways may be regulating these responses, with MPTP formation likely playing a significant role.

To further ascertain the difference between the cellular effects of CBD and AO, we compared the ability of CsA to alleviate mitochondrial depolarization from CBD or AO. Once again, AO and CBD decreased mitochondrial polarization compared to vehicle at 2 h (Fig. 4E, blue bars). CsA had no effect on depolarization by AO. In contrast, CBD-treated cells decreased TMRE signal to 39.8% of baseline but only 71.9% with CsA present (Fig. 4F, gray bars). This recovery of mitochondrial depolarization, although partial, is to our knowledge a novel phenotype not seen in other attempts to inhibit AO effects or Parkin signaling. Collectively, these results indicate that CBD modulates the PINK1/Parkin pathway in a distinct manner from AO or any known activators of PINK1 and Parkin.

2.6. CBD generates Parkin-positive mitochondrial-derived vesicles

The dynamics of CBD-induced PINK1/Parkin activation share some similarities with Antimycin A treatment in the absence of Oligomycin A. Previous studies showed that Antimycin A treatment alone can induce the production of mitochondrial-derived vesicles (MDV), which are cargo-selective vesicles that selectively degrade mitochondrial fragments in a process distinct from the mitophagy seen after CCCP treatment (McLelland et al., 2014). Processing of injured mitochondria via MDV formation is distinct from CCCP-induced mitophagy. To test if CBD induces this repair pathway through MDV formation, we treated RPE1 cells expressing Venus-Parkin with CCCP, Antimycin A, or CBD, and then fixed and stained these cells with antibodies against TOM20, an outer mitochondrial membrane protein, or PDH2/3, which reside within the mitochondrial matrix. To measure MDV production, we first located distinct Parkin puncta within cells small enough to viably be classified as

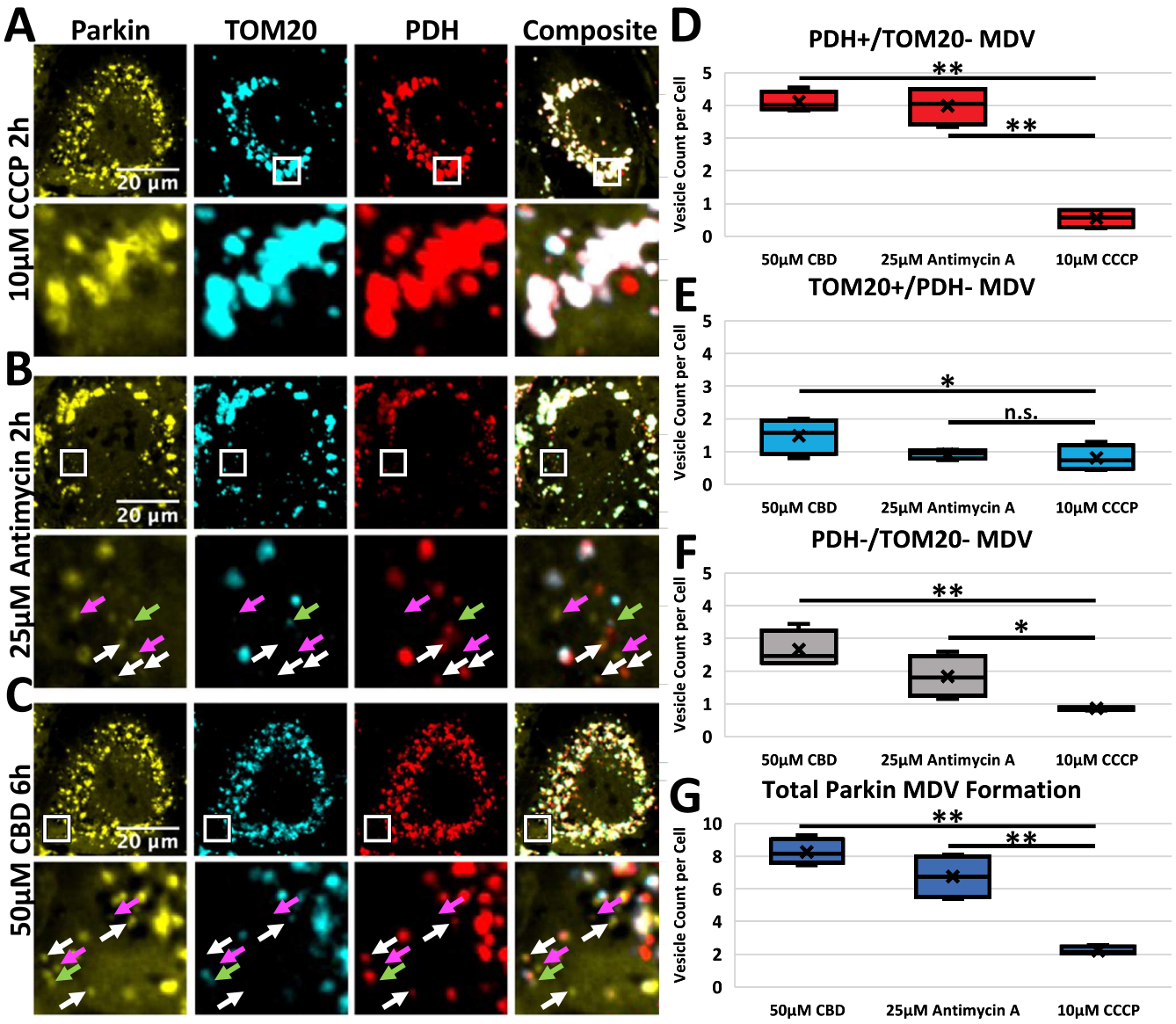

Fig. 5. CBD Induces MDV Formation. A-B) RPE1 cells expressing Venus-Parkin (yellow) were treated with 10 μM CCCP (top row), 25 μM Antimycin for 2 h (middle row), or 50 μM CBD for 6 h (bottom row), then fixed and stained for TOM20 (blue) and PDH (red). Top row of each treatment is full image, bottom row is inset of boxed area. White arrow: PDH+/ TOM20- MDV. Green Arrow: TOM20+/PDH- MDV. Pink Arrow: PDH-/TOM20- MDV, D-G) Quantification of Parkin puncta vesicles containing PDH but absent TOM20 (D), TOM20 but absent PDH (E), absent TOM20 and PDH (F), and total MDV formation (G). *t*-test comparing CBD or AO to CCCP treatment represented as p-value < .005 = **, p-value < .05 = *, n.s. = not significant, n = 20 cells per replicate, 4 replicates.

MDVs using light microscopy (< ~ 1 μm). From these small Parkin puncta, we then counted the number of puncta selective for TOM20 (TOM20+/PDH-), PDH (PDH+/TOM20-) or excluding both markers (PDH-/TOM20-). 20 cells per sample were counted and averaged for vesicle counts. CBD treatment stimulated formation of all three types of MDVs (Fig. 5C, white arrows: PDH+/TOM20-, green arrow: TOM20-/PDH+, pink arrow: PDH-/TOM20-). This formation is also seen in Antimycin A-treated cells, while CCCP treatment causes almost no MDV formation (Fig. 5B and A, respectively). Quantification reveals that both CBD and Antimycin A caused cells to generate significantly more PDH+/TOM20- MDVs and overall MDVs than CCCP (Fig. 5D and G, respectively), while CBD alone caused increased production of PDH-/TOM20- MDVs (Fig. 5F). Statistically, there was no difference in TOM20+/PDH- MDVs across the three treatments (Fig. 5E). This shows that CBD induces MDV formation comparably to Antimycin A treatment.

3. Discussion

Here we describe our findings that CBD activates the PINK1-Parkin pathway in a dose-dependent manner, leading both to mitochondrial clearance and to elevated production of MDVs. CBD causes PINK1 to stabilize on the mitochondrial membrane and Parkin to be recruited to damaged mitochondria while simultaneously inducing mitochondrial depolarization and ROS production similarly to AO or CCCP. However, the underlying mechanism appears to be distinct from the mechanisms of AO and CCCP because cyclosporine A can inhibit the PINK1/Parkin activity of CBD, while having no discernable effect on Parkin recruitment in cells treated with AO. While CBD-induced activation of Parkin leads to autophagosome recruitment and mitophagy in a manner similar to AO, it also elevates generation of MDVs. Thus, our studies uncover a novel and clinically relevant inducer of MDVs and describe a new mechanism of action by which CBD regulates cellular responses.

Several small molecules have been shown to activate the PINK1/Parkin pathway via mechanisms of action that can be classified into three distinct classes. CCCP, FCCP, and valinomycin depolarize mitochondria by perturbing ion flux across the membranes (Narendra et al., 2008; Zhang et al., 2014). The second class includes AO and sorafenib, which inhibit complex III and V of the electron transport chain (ETC), leading to ROS generation and depolarization (Vives-Bauza et al., 2010; Zhang et al., 2017). Actinonin and G-TTP belong to the third class that are known to cause misfolded protein accumulation at mitochondria in a manner similar to overexpression of truncated OTC, leaving them polarized during Parkin recruitment (Burman et al., 2017; Fiesel et al., 2017; Jin and Youle, 2013). While CBD causes some cellular effects that are similar to those caused by these previously defined PINK1/Parkin activators, its underlying mechanism may be distinct. A recent paper by Huang, et al. presented work that CBD induced Parkin-dependent mitophagy, leading to cell death in glioma cells (Huang et al., 2021). We demonstrate that CsA selectively blocks PINK1/Parkin activation caused by CBD. In contrast, CsA does not negate PINK1-Parkin activation by CCCP, valinomycin, or AO. CsA can even sensitize cells to actinonin, which leads to increased Parkin puncta formation (Fig. S6). CBD does cause mitochondrial depolarization (Fig. 2A), but the kinetics of depolarization are slower than those after treatment with CCCP or AO. Thus, the cellular response to co-treatment with CsA differentiates CBD from the three known types of PINK1-Parkin inducers.

Previous studies showed that CBD causes mitochondrial Ca^{2+} overload and stable mitochondrial permeability transition pore (MPTP) formation, which could be responsible for mitochondrial depolarization (Olivas-Aguirre et al., 2019). Consistent with this hypothesis, CsA reverses CBD-induced depolarization but has no effect on AO-induced depolarization. CsA is known to obstruct MPTP formation via binding to CypD (Bernardi et al., 1994; Crompton et al., 1988). Indeed our research suggests that CypD directly functions during this Parkin-mediated mitochondrial stress response to CBD. CsA has been shown previously to block the calcium flux caused by CBD, protecting cells from the subsequent cytotoxic effects (Olivas-Aguirre et al., 2019). The calcium influx or overloading caused by CBD leading to MPTP opening could be responsible for the Parkin recruitment. Another relevant mechanism could be attributed to inhibition of complex II/III and slow mitochondrial depolarization by CBD (Singh et al., 2015). Since CsA does not reverse AO-induced mitochondrial depolarization, ETC complex inhibition by CBD is unlikely to be the major cause of PINK1-Parkin activation. Given both mitochondrially targeted CsA and knockdown of CypD significantly perturb the effect of CBD, our findings instead are in line with previous work showing that CBD promotes MPTP formation. Future studies will be needed to test whether MPTP formation is directly responsible for PINK1/Parkin activity and whether additional pathways are required in addition to MPTP activation to mediate CBD effects.

MDVs provide an alternative to mitophagy for processing damaged mitochondria recognized by Parkin (Sugiura et al., 2014). This pathway is selective in its cargo, shown to package oxidized proteins (Soubannier et al., 2012b). The key defining feature of these vesicles is the selective packaging of mitochondrial proteins. MDVs have been shown either carrying matrix proteins while excluding OMM proteins, or vice versa (McLelland et al., 2014; Ryan et al., 2020). These MDVs are then trafficked to the lysosome to be degraded (Soubannier et al., 2012a). Compared to the extensive destruction of whole organelles during mitophagy, MDV formation and processing present a less drastic form of mitochondrial maintenance. Repairing minor stress with MDVs could act as a safeguard from triggering mitophagy, which could be seen as the nuclear option for cells dealing with stressed mitochondria. CBD caused slower Parkin and PINK1 recruitment, depolarization, and superoxide production than AO treatment. This more gradual accumulation of mitochondria damage could be the driving force behind this MDV formation. The fact that we see significant MDV formation only at this relatively high dose might be due to the transient nature of these vesicles. Lower doses of CBD might be inducing a smaller amount of Parkin-dependent MDVs that are degraded before noticeable accumulation occurs. Consistent with notion, bafilomycin treatment enhances Parkin colocalization to mitochondria at lower doses of CBD (Fig. S7). A small amount of induced MDV formation could help cells better process mitochondrial damage before mitophagy is needed and explain the proliferative effects seen in low dose treatment of CBD (Olivas-Aguirre et al., 2019). This increased activation of controlled mitochondrial maintenance could offer beneficial benefits to these treated cells.

CBD is being explored in the clinic as a remedy for several neurodegenerative disorders, including epilepsy and Parkinson's disease. Although some initial results are promising, a myriad of questions remain about the detrimental and beneficial effects that CBD exerts on cells. Previous research provided a frame work for CBD induced Parkin-dependent mitophagy (Huang et al., 2021). This work shows that at micromolar range, CBD exhibits mitocan effects, impairment of mitochondria, and activation of the PINK1/Parkin repair pathway, possibly through the opening of the MPTP. Since mitochondria dysfunction is linked to a wide swath of neurological diseases, further elucidating this signaling pathway could provide promising insights to CBD's value as a therapeutic agent.

4. Methods

4.1. Cell culture, transfection, and reagent treatment

HEK293T cells were obtained from ATCC. HeLa cells were a gifted by Sabrina Spencer. Beige fat cells were a gift from Shingo Kajimura. Cells were maintained in Dulbecco's Modified Eagle's Medium (DMEM) supplemented with 10% fetal calf serum (Invitrogen), penicillin, streptomycin (100units/mL), and 1 mM L-glutamine. Cells were treated at indicated concentrations with CCCP (SigmaAldrich), valinomycin (Tocris), Antimycin (SigmaAldrich) Oligomycin (Cayman Chemical), Actinonin (Cayman Chemical), FK506 (Cayman Chemical), 1-NA-PP1

(Cayman Chemical), Bafilomycin A1 (SigmaAldrich), and Ru360 (EMDMillipore). Antibodies were purchased from the following providers: anti-PDH, Abcam; anti-Tom20, Proteintech. Fluorescent labeled secondary antibodies were purchased from ThermoFisher.

4.2. Generation of shRNA knockdown cell lines

pLKO.1 lentiviral vectors were obtained from the Functional Genomics Facility at CU Cancer Center. HEK293T cells were transfected with lentiviral packaging and target plasmids to generate lentivirus, and viral supernatants were collected and filtered before infecting into target cells. Cells were then selected with puromycin. CypD (TRCN0000232682) targeting sequence: CCGGGTTCTTCATCTGCACCATAAACTCGAGTTTATGGTGCAGATGAAGAACTTTTTG. qPCR analysis of CypD knockdown was performed with the following pair of primers: Fwd 5′-GAAGGCAGATGTCGTCCCAAA-3′; Rev 5′-GGAAAGCGGCTTCCGTAGAT-3′. Human TBP was used as an internal control for the normalization of sample inputs. The primer pair for TBP are: Fwd 5′- CACGAACCACGGCACTGATT-3′; Rev 5′-TTTTCTTGCTGCCAGTCTGGAC-3′.

4.3. Live cell imaging and fluorescence microscopy

For Parkin recruitment and mitophagy assays, cells were grown in Perkin Elmer Cell Carrier Ultra 96-well plates at 5000 cells per well at 37°C and 5% CO_2 in a humidified incubator. Cells were imaged at 5% CO2 and 37°C in a Perkin Elmer Opera Phenix High-Content Screening System with the laser and filter settings for CFP, YFP, and mCherry using a 40x water NA 1.1 objective. Live cell images were collected for 0–22 h post-treatment.

For PINK1 stabilization and mitochondrial membrane potential assays, 5000 cells per well were grown in Cell Carrier Ultra 96-well plates at 37 °C and 5% CO_2 in a humidified incubator. Cells were imaged at 5% CO2 and 37 °C in a Perkin Elmer Opera Phenix High-Content Screening System with the laser and filter settings for EGFP and TRITC using a 20x Air NA.8 objective. Live cell images were collected for a pre-treatment time point and 0–8 h after treatment.

4.4. Parkin mitochondrial recruitment assays

Parkin mitochondrial translocation was calculated two ways: Parkin puncta formation and Parkin colocalization to mitochondria: (1) Venus-Parkin and Smac-MTS-RFP (mitochondrial intermembrane space marker) or immunostain Tom20 (outer mitochondrial protein) were imaged using the Opera Phenix, then images were quantified using the Harmony analysis suite. Images were masked for areas positive for Smac-MTS-RFP. The count of YFP puncta was then recorded for each image in a time series and normalized to the count for the first time point for each site; (2) The Venus-Parkin and Smac-MTS-RFP images were analyzed in MATLAB. Images underwent background subtraction and thresholding before the Pearson's Correlation Coefficient was calculated for each site and averaged across wells and replicates.

4.5. Mitophagy assays

Mitophagy was quantified using co-localization experiments between LC3 and mitochondria (Smac-MTS-RFP). MATLAB was used to process images using background subtraction and thresholding before a Pearson's Correlation Coefficient was calculated for each site and averaged across wells and replicates.

4.6. PINK1 stabilization assay

PINK1-EGFP stabilization was quantified using MATLAB to background subtract and threshold images. Average EGFP pixel intensity was calculated for each image. For each time point, values were normalized to the pre-treatment value for the corresponding site.

4.7. Mitochondrial membrane potential assay and quantification

Mitochondria were stained with TMRE dye (ThermoFisher) as described previously (Zhang et al., 2017). Cells were imaged for 20 ms at 20% power using the TRITC filter on the Opera Phenix. Membrane potential was quantified by using MATLAB to background subtract and threshold images. Average TRITC pixel intensity was calculated for each image. For each time point, values were normalized to the pre-treatment value for the corresponding site.

4.8. Mitochondrial superoxide production assay

Mitochondria were stained with MitoSox dye (ThermoFisher) following the protocols provided by the manufacturer. Cells were then treated with drugs for the indicated length. Cells were then fixed with 4% PFA, stained with a Tom20 primary antibody, and stained with an Alexa647 secondary antibody. Cells were imaged for 100 ms at 50% power using the TRITC and Alexa647 settings on the Opera Phenix. Membrane potential was quantified by using MATLAB to background subtract and threshold images. Average TRITC and Alexa647 pixel intensity were calculated for each image.

4.9. Mitochondria morphological change

HeLa cells with Venus-Parkin and Smac-MTS-RFP were incubated with 1 μM Draq5 (Invitrogen) as suggested by the manufacturer for 20 min, and then treated as indicated. Cells were then imaged on the Opera Phenix for 100 ms at 40% power for both mCherry and Draq5 signal. Images were then analyzed for mitochondrial morphology using the SER hole feature of the PerkinElmer Harmony analysis suite according to the guidelines provided by PerkinElmer.

4.10. Measuring mitochondrial content change

HeLa cells with Smac-MTS-RFP were treated with indicated drugs and imaged for 16 h. After flatfield correction and background subtraction images were calculated for intensity of RFP fluorescence in MATLAB. Fluorescence at 16 h was normalized to the initial time measurement for each well and then averaged across separate experiments.

4.11. Immunofluorescence and MDV formation quantification

RPE1 cells expressing Venus-Parkin were treated as indicated and then fixed with 6% PFA in PBS for 15 min, then washed with PBS. Cells were blocked and permeabilized with 1% BSA and.3% Triton-X 100 for 1 h, then incubated with mouse anti-PDH2/2 (1:1000, Abcam, ab110333) and rabbit anti-TOM20 (1:250, Cell Signaling, 42406) antibodies overnight at 4 °C. Cells were washed with PBS and then incubated with Alexa 555 anti-rabbit (1:250, Invitrogen, A27039) and Alex 647 anti-mouse (1:250, Invitrogen, A32728) for 1 h at room temperature. Cells were washed, then imaged on the Opera Phenix using the YFP, TRITC, and Cy5 filters.

MDV formation was quantified by identifying Parkin puncta that had no TOM20 or PDH2/3 expression. TOM20+/PDH2/3-, PDH2/3+/TOM20-, and double negative Parkin puncta were counted for 20 cells per replicate, with 2 technical and 2 biological replicates for each condition.

4.12. Statistics

All statistical data was calculated using MATLAB or Excel. Comparisons between individual conditions were performed using a two-sample *t*-test with one-tailed distribution and unequal variance. *p*-values < 0.05

were marked as *, and p-values < 0.005 were marked as **.

Acknowledgments

We thank Dr. Joseph Dragavon and the BioFrontiers Advanced Light Microscopy Core for their microscopy support. We thank Shingo Kajimura for sharing the beige adipocyte cells. This work was supported by grants from the National Institute of Arthritis and Musculoskeletal and Skin Diseases and the National Institute of General Medicine of the National Institutes of Health (R01AR068254 and R01GM113141 to Xuedong Liu) and National Institute of General Medical Sciences (NIGMS) R01GM135592 to Hao Bing. A.R. was supported by a predoctoral training grant from the National Institute of General Medical Sciences (T32GM08759) and Diversity Supplement (R01AR068254-S1). The content is solely the responsibility of the authors and does not necessarily represent the official views of the National Institutes of Health. The ImageXpress MicroXL imaging system was supported by NCRR S10RR026680, the BDAria cell sorter by S10OD021601, the Opera Phenix imaging system by S10OD025072 from NIH.

Appendix A. Supplementary material

Supplementary data associated with this article can be found in the online version at doi:10.1016/j.ejcb.2021.151185.

References

Bernardi, P., Broekemeier, K.M., Pfeiffer, D.R., 1994. Recent progress on regulation of the mitochondrial permeability transition pore; a cyclosporin-sensitive pore in the inner mitochondrial membrane. J. Bioenerg. Biomembr. 26, 509–517. https://doi.org/10.1007/BF00762735.

Boland, M.L., Chourasia, A., Macleod, K.F., 2013. Mitochondrial dysfunction in cancer. Front. Oncol. 3, 292. https://doi.org/10.3389/fonc.2013.00292.

Burman, J.L., Pickles, S., Wang, C., Sekine, S., Vargas, J.N.S., Zhang, Z., Youle, A.M., Nezich, C.L., Wu, X., Hammer, J.A., Youle, R.J., 2017. Mitochondrial fission facilitates the selective mitophagy of protein aggregates. J. Cell Biol. 216, 3231–3247. https://doi.org/10.1083/jcb.201612106.

Carroll, R.G., Hollville, E., Martin, S.J., 2014. Parkin sensitizes toward apoptosis induced by mitochondrial depolarization through promoting degradation of Mcl-1. Cell Rep. 9, 1538–1553. https://doi.org/10.1016/j.celrep.2014.10.046.

Chistiakov, D.A., Shkurat, T.P., Melnichenko, A.A., Grechko, V., Orekhov, A.N., 2017. The role of mitochondrial dysfunction in cardiovascular disease: a brief review. Ann. Med. 50, 121–127 https://doi.org/07853890.2017.1417631.

Crompton, M., Ellinger, H., Costi, A., 1988. Inhibition by cyclosporin A of a Ca2+-dependent pore in heart mitochondria activated by inorganic phosphate and oxidative stress. Biochem. J. 255, 357–360.

Devinsky, O., Cross, J.H., Laux, L., Marsh, E., Miller, I., Nabbout, R., Scheffer, I.E., Thiele, E.A., Wright, S., 2017. Trial of cannabidiol for drug-resistant seizures in the dravet syndrome. N. Engl. J. Med. 376, 2011–2020. https://doi.org/10.1056/NEJMoa1611618.

Fiesel, F.C., James, E.D., Hudec, R., Springer, W., 2017. Mitochondrial targeted HSP90 inhibitor Gamitrinib-TPP (G-TPP) induces PINK1/Parkin-dependent mitophagy. Oncotarget 8, 106233–106248. https://doi.org/10.18632/oncotarget.22287.

Greene, A.W., Grenier, K., Aguileta, M.A., Muise, S., Farazifard, R., Haque, M.E., McBride, H.M., Park, D.S., Fon, E.A., 2012. Mitochondrial processing peptidase regulates PINK1 processing, import and Parkin recruitment. EMBO Rep. 13, 378–385. https://doi.org/10.1038/embor.2012.14.

Hao, E., Mukhopadhyay, P., Cao, Z., Erdélyi, K., Holovac, E., Liaudet, L., Lee, W.-S., Haskó, G., Mechoulam, R., Pacher, P., 2015. Cannabidiol protects against doxorubicin-induced cardiomyopathy by modulating mitochondrial function and biogenesis. Mol. Med. 21, 38–45. https://doi.org/10.2119/molmed.2014.00261.

Huang, T., Xu, T., Wang, Y., Zhou, Y., Yu, D., Wang, Z., He, L., Chen, Z., Zhang, Y., Davidson, D., Dai, Y., Hang, C., Liu, X., Yan, C., 2021. Cannabidiol inhibits human glioma by induction of lethal mitophagy through activating TRPV4. Autophagy 1–15. https://doi.org/10.1080/15548627.2021.1885203.

Jin, S.M., Lazarou, M., Wang, C., Kane, L.A., Narendra, D.P., Youle, R.J., 2010. Mitochondrial membrane potential regulates PINK1 import and proteolytic destabilization by PARL. J. Cell Biol. 191, 933–942. https://doi.org/10.1083/jcb.201008084.

Jin, S.M., Youle, R.J., 2013. The accumulation of misfolded proteins in the mitochondrial matrix is sensed by PINK1 to induce PARK. Autophagy 9, 1750–1757. https://doi.org/10.4161/auto.26122.

Klein, C., Westenberger, A., 2012. Genetics of Parkinson's disease. Cold Spring Harb. Perspect. Med. 2, 008888 https://doi.org/10.1101/cshperspect.a008888.

Leehey, M.A., Liu, Y., Hart, F., Epstein, C., Cook, M., Sillau, S., Klawitter, J., Newman, H., Sempio, C., Forman, L., Seeberger, L., Klepitskaya, O., Baud, Z., Bainbridge, J., 2020. Safety and tolerability of cannabidiol in parkinson disease: an open label, dose-escalation study. Cannabis Cannabinoid Res. 5, 326–336. https://doi.org/10.1089/can.2019.0068.

Matsuda, N., Sato, S., Shiba, K., Okatsu, K., Saisho, K., Gautier, C.A., Sou, Y., Saiki, S., Kawajiri, S., Sato, F., Kimura, M., Komatsu, M., Hattori, N., Tanaka, K., 2010. PINK1 stabilized by mitochondrial depolarization recruits Parkin to damaged mitochondria and activates latent Parkin for mitophagy. J. Cell Biol. 189, 211–221. https://doi.org/10.1083/jcb.200910140.

McLelland, G.-L., Soubannier, V., Chen, C.X., McBride, H.M., Fon, E.A., 2014. Parkin and PINK1 function in a vesicular trafficking pathway regulating mitochondrial quality control. EMBO J. 33, 282–295. https://doi.org/10.1002/embj.201385902.

Narendra, D., Tanaka, A., Suen, D.-F., Youle, R.J., 2008. Parkin is recruited selectively to impaired mitochondria and promotes their autophagy. J. Cell Biol. 183, 795–803. https://doi.org/10.1083/jcb.200809125.

Narendra, D.P., Jin, S.M., Tanaka, A., Suen, D.-F., Gautier, C.A., Shen, J., Cookson, M.R., Youle, R.J., 2010. PINK1 Is selectively stabilized on impaired mitochondria to activate Parkin. PLoS Biol. 8, e1000298 https://doi.org/10.1371/journal.pbio.1000298.

Olivas-Aguirre, M., Torres-López, L., Valle-Reyes, J.S., Hernández-Cruz, A., Pottosin, I., Dobrovinskaya, O., 2019. Cannabidiol directly targets mitochondria and disturbs calcium homeostasis in acute lymphoblastic leukemia. Cell Death Dis. 10, 779. https://doi.org/10.1038/s41419-019-2024-0.

Ordureau, A., Paulo, J.A., Zhang, J., An, H., Swatek, K.N., Cannon, J.R., Wan, Q., Komander, D., Harper, J.W., 2020. Global landscape and dynamics of Parkin and USP30-dependent ubiquitylomes in ineurons during mitophagic signaling. Mol. Cell 77, 1124–1142. https://doi.org/10.1016/j.molcel.2019.11.013 e10.

Pawlyk, A.C., Giasson, B.I., Sampathu, D.M., Perez, F.A., Lim, K.L., Dawson, V.L., Dawson, T.M., Palmiter, R.D., Trojanowski, J.Q., Lee, V.M.-Y., 2003. Novel monoclonal antibodies demonstrate biochemical variation of brain Parkin with age. J. Biol. Chem. 278, 48120–48128. https://doi.org/10.1074/jbc.M306889200.

Pickrell, A.M., Youle, R.J., 2015. The roles of PINK1, Parkin, and mitochondrial fidelity in Parkinson's disease. Neuron 85, 257–273. https://doi.org/10.1016/j.neuron.2014.12.007.

Rimmerman, N., Ben-Hail, D., Porat, Z., Juknat, A., Kozela, E., Daniels, M.P., Connelly, P.S., Leishman, E., Bradshaw, H.B., Shoshan-Barmatz, V., Vogel, Z., 2013. Direct modulation of the outer mitochondrial membrane channel, voltage-dependent anion channel 1 (VDAC1) by cannabidiol: a novel mechanism for cannabinoid-induced cell death. Cell Death Dis. 4, 949. https://doi.org/10.1038/cddis.2013.471 e949–e949.

Roberts, R.F., Tang, M.Y., Fon, E.A., Durcan, T.M., 2016. Defending the mitochondria: the pathways of mitophagy and mitochondrial-derived vesicles. Int. J. Biochem. Cell Biol. 79, 427–436. https://doi.org/10.1016/j.biocel.2016.07.020.

Ryan, T.A., Phillips, E.O., Collier, C.L., JB Robinson, A., Routledge, D., Wood, R.E., Assar, E.A., Tumbarello, D.A., 2020. Tollip coordinates Parkin-dependent trafficking of mitochondrial-derived vesicles. EMBO J. 39, 102539 https://doi.org/10.15252/embj.2019102539.

Sarraf, S.A., Raman, M., Guarani-Pereira, V., Sowa, M., Huttlin, E.L., Gygi, S.P., Harper, J.W., 2013. Landscape of the PARKIN-dependent ubiquitylome in response to mitochondrial depolarization. Nature 496, 372–376. https://doi.org/10.1038/nature12043.

Singh, N., Hroudová, J., Fišar, Z., 2015. Cannabinoid-induced changes in the activity of electron transport chain complexes of brain mitochondria. J. Mol. Neurosci. 56, 926–931. https://doi.org/10.1007/s12031-015-0545-2.

Soubannier, V., McLelland, G.-L., Zunino, R., Braschi, E., Rippstein, P., Fon, E.A., McBride, H.M., 2012a. A vesicular transport pathway shuttles cargo from mitochondria to lysosomes. Curr. Biol. 22, 135–141. https://doi.org/10.1016/j.cub.2011.11.057.

Soubannier, V., Rippstein, P., Kaufman, B.A., Shoubridge, E.A., McBride, H.M., 2012b. Reconstitution of mitochondria derived vesicle formation demonstrates selective enrichment of oxidized cargo. PLoS ONE 7, e52830. https://doi.org/10.1371/journal.pone.0052830.

Sugiura, A., McLelland, G., Fon, E.A., McBride, H.M., 2014. A new pathway for mitochondrial quality control: mitochondrial-derived vesicles. EMBO J. 33, 2142–2156. https://doi.org/10.15252/embj.201488104.

Thiele, E.A., Marsh, E.D., French, J.A., Mazurkiewicz-Beldzinska, M., Benbadis, S.R., Joshi, C., Lyons, P.D., Taylor, A., Roberts, C., Sommerville, K., Gunning, B., Gawlowicz, J., Lisewski, P., Mazurkiewicz Beldzinska, M., Mitosek Szewczyk, K., Steinborn, B., Zolnowska, M., Hughes, E., McLellan, A., Benbadis, S., Ciliberto, M., Clark, G., Dlugos, D., Filloux, F., Flamini, R., French, J., Frost, M., Haut, S., Joshi, C., Kapoor, S., Kessler, S., Laux, L., Lyons, P., Marsh, E., Moore, D., Morse, R., Nagaraddi, V., Rosenfeld, W., Seltzer, L., Shellhaas, R., Sullivan, J., Thiele, E., Thio, L.L., Wang, D., Wilfong, A., 2018. Cannabidiol in patients with seizures associated with Lennox-Gastaut syndrome (GWPCARE4): a randomised, double-blind, placebo-controlled phase 3 trial. Lancet 391, 1085–1096. https://doi.org/10.1016/S0140-6736(18)30136-3.

Valvassori, S.S., Bavaresco, D.V., Scaini, G., Varela, R.B., Streck, E.L., Chagas, M.H., Hallak, J.E.C., Zuardi, A.W., Crippa, J.A., Quevedo, J., 2013. Acute and chronic administration of cannabidiol increases mitochondrial complex and creatine kinase activity in the rat brain. Rev. Bras. Psiquiatr. 35, 380–386. https://doi.org/10.1590/1516-4446-2012-0886.

Vives-Bauza, C., Zhou, C., Huang, Y., Cui, M., de Vries, R.L.A., Kim, J., May, J., Tocilescu, M.A., Liu, W., Ko, H.S., Magrane, J., Moore, D.J., Dawson, V.L., Grailhe, R., Dawson, T.M., Li, C., Tieu, K., Przedborski, S., 2010. PINK1-dependent recruitment of Parkin to mitochondria in mitophagy. Proc. Natl. Acad. Sci. 107, 378–383. https://doi.org/10.1073/pnas.0911187107.

Warne, J., Pryce, G., Hill, J.M., Shi, X., Lennerås, F., Puentes, F., Kip, M., Hilditch, L., Walker, P., Simone, M.I., Chan, A.W.Edit, Towers, G.J., Coker, A.R., Duchen, M.R., Szabadkai, G., Baker, D., Selwood, D.L., 2016. Selective inhibition of the

mitochondrial permeability transition pore protects against neurodegeneration in experimental multiple sclerosis. J. Biol. Chem. 291, 4356–4373. https://doi.org/10.1074/jbc.M115.700385.

Yamano, K., Matsuda, N., Tanaka, K., 2016. The ubiquitin signal and autophagy: an orchestrated dance leading to mitochondrial degradation. EMBO Rep. 17, 300–316. https://doi.org/10.15252/embr.201541486.

Yeung, R.O., Al Jundi, M., Gubbi, S., Bompu, M.E., Sirrs, S., Tarnopolsky, M., Hannah-Shmouni, F., 2021. Management of mitochondrial diabetes in the era of novel therapies. J. Diabetes Complicat. 35, 107584 https://doi.org/10.1016/j.jdiacomp.2020.107584.

Yoshii, S.R., Kishi, C., Ishihara, N., Mizushima, N., 2011. Parkin mediates proteasome-dependent protein degradation and rupture of the outer mitochondrial membrane. J. Biol. Chem. 286, 19630–19640. https://doi.org/10.1074/jbc.M110.209338.

Zhang, C., Lee, S., Peng, Y., Bunker, E., Giaime, E., Shen, J., Zhou, Z., Liu, X., 2014. PINK1 triggers autocatalytic activation of Parkin to specify cell fate decisions. Curr. Biol. 24, 1854–1865. https://doi.org/10.1016/j.cub.2014.07.014.

Zhang, C., Lee, S., Peng, Y., Bunker, E., Shen, C., Giaime, E., Shen, Jie, Shen, Jingshi, Zhou, Z., Liu, X., 2015. A chemical genetic approach to probe the function of PINK1 in regulating mitochondrial dynamics. Cell Res. 25, 394–397. https://doi.org/10.1038/cr.2014.159.

Zhang, C., Liu, Z., Bunker, E., Ramirez, A., Lee, S., Peng, Y., Tan, A.-C., Eckhardt, S.G., Chapnick, D.A., Liu, X., 2017. Sorafenib targets the mitochondrial electron transport chain complexes and ATP synthase to activate the PINK1–Parkin pathway and modulate cellular drug response. J. Biol. Chem. 292, 15105–15120. https://doi.org/10.1074/jbc.M117.783175.